

Supporting Information

Host-Guest Strategy for Converting the Photodynamic Agents from Singlet Oxygen Generator to Superoxide Radical Generator

Kun-Xu Teng, Li-Ya Niu and Qing-Zheng Yang*

Key Laboratory of Radiopharmaceuticals, Ministry of Education, College of Chemistry, Beijing Normal University, Beijing 100875, P. R. China.

Email: qzyang@bnu.edu.cn

Table of Contents

1. General information.....	S2
2. Synthesis of BP5A and G	S5
3. The ¹ H NMR and 2D NMR spectroscopy of HG	S7
4. The preparation and morphological properties of HG	S12
5. The photophysical and photochemical properties of HG	S14
6. The evaluation of ROS generation ability.....	S15
7. The characteristics of the aggregates of G and ROS generation ability.....	S18
8. The electrochemical properties of G and BP5A	S20
9. Experimental data <i>in vitro</i> and <i>in vivo</i>	S21
10. NMR spectra and HRMS.....	S23
11. Reference.....	S27

1. General information

1) Materials and Instruments

Unless otherwise mentioned, materials were obtained from commercial suppliers and were used without further purification. All reactions were performed in dry glassware (Hinwil). Column chromatography was performed over silica gel (200-300 mesh). NMR spectra were recorded with JEOL-400, JEOL-600 or Bruker Avance 700 spectrometers. High-resolution mass spectrometry experiments were recorded by Bruker Solarix XR Fourier Transform Ion Cyclotron Resonance Mass Spectrometer. Absorption spectra of liquid samples were determined on Hitachi UV-3900 spectrophotometer at room temperature. Fluorescence spectra of liquid samples were determined on Hitachi F-4600 spectrophotometer at room temperature. Dynamic light scattering (DLS) investigations were carried out with a DynaPro NanoStar dynamic light scattering detector. Scanning electron microscope (SEM) images were obtained using a Hitachi SU-8010 instrument. The photostability was conducted under irradiation with a high-power LED light and monitored by using an UV-3900 spectrophotometer. Electron spin resonance was performed with Bruker E500. Confocal fluorescence imaging was performed with Nikon A1R microscopy. Cell viability test was obtained on a Thermo Scientific Multiskan. Irradiation was performed by using a LED light (660 nm, PLS-LED 100, Perfect Light, Beijing, China). *In vivo* imaging was recorded by an IVIS Spectrum imaging system (PerkinElmer, USA). All mouse models are provided by Beijing Vital River Laboratory Animal Technology Co., Ltd.

2) Ethical statement

Procedures related to animal experiments were implemented in compliance with the China Animal Management Regulations (2017 Edition), and were approved by the animal care committee of Beijing Normal University.

3) Detection of $^1\text{O}_2$ production in solution

Compound 9,10-anthracenediyl-bis(methylene)-dimalonic acid (ABDA) was used as indicator for detection of $^1\text{O}_2$ in solution (Figure S11). 10 μM of photosensitizer was dissolved in 2 mL solution containing 30 μM of ABDA. The mixture was then placed in a cuvette and irradiated with a 660 nm LED light at 20 mW cm^{-2} . The absorption change of sample at 378 nm was recorded by the UV-Vis absorption spectrophotometer.

4) Detection of $\text{O}_2^{\cdot-}$ production with DHE in solution

Droethidium (DHE) was used as indicator for detection of $\text{O}_2^{\cdot-}$ in solution. When $\text{O}_2^{\cdot-}$ is generated in the system, DHE can be oxidized to form ethidium which intercalates into DNA and emits bright fluorescence at ~ 580 nm (Figure S12). 10 μM of photosensitizer was dissolved/dispersed in 2 mL PBS containing 40 μM of DHE and 500 $\mu\text{g/mL}$ ctDNA. The mixture was then placed in a cuvette and irradiated with a 660 nm LED light at 20 mW cm^{-2} . The fluorescence change of sample was recorded by the fluorescence spectrometer.

5) Detection of ROS production in solution

Compound 2',7'-dichlorodihydrofluorescein (DCFH) was used as indicator for detection of ROS in solution (Figure S13). 10 μM of photosensitizer was dissolved in 2 mL solution

containing 40 μM of DCFH. The mixture was then placed in a cuvette and irradiated with a 660 nm LED light at 20 mW cm^{-2} . The fluorescence intensity change of the sample at 522 nm in PBS or 550 nm in DMF was recorded by the fluorescence spectrometer.

6) The photodegradation experiment of rhodamine B

The rhodamine B (RhB) was employed to study the kinetic of ROS generation of **HG**. 10 μM RhB was dissolved in 2 mL water containing 20 μM of **HG**. The mixture was then placed in a cuvette and irradiated with a 660 nm LED light at 20 mW cm^{-2} . The absorption change of sample at 550 nm was recorded by the UV-Vis absorption spectrophotometer.

7) Detection of $\text{O}_2^{\cdot-}$ production with ESR spectroscopy

BMPO was used as a spin trap for detection of $\text{O}_2^{\cdot-}$ by ESR spectroscopy in water or DMSO. Electron spin resonance (ESR) spectroscopy was employed to detect the ESR signals of the following five groups of samples: i) 100 μM of **HG** was dispersed in water containing 25 mM of BMPO and illuminated with a xenon lamp; ii) 100 μM of **G** was dissolved in DMSO containing 25 mM of BMPO and illuminated with a xenon lamp; iii) 100 μM of **HG** was dispersed in water containing 25 mM of BMPO without light; iv) 100 μM of **G** was dissolved in DMSO containing 25 mM of BMPO without light; v) 25 mM of BMPO was dissolved in DMSO and illuminated with a xenon lamp.

8) Cyclic Voltammetry Measurement

Cyclic voltammograms experiment was conducted by using three-electrode system. A glassy-carbon electrode was used as working electrode, the Pt wire electrode and the Ag/Ag^+ electrode were used as the auxiliary electrode and reference electrode, respectively. The measurement was conducted in dichloromethane containing 0.1 M tetrabutylammonium hexafluorophosphate. The scan rate was optimized as 100 mV/s . Fc/Fc^+ was used as external reference.

9) ROS generation in living cells

HeLa cells were seeded in 35 mm confocal dishes and incubated for 24 hours under normoxia or hypoxia. Specifically, the HeLa cells were incubated with 0.5 μM **HG** at 37 $^\circ\text{C}$ for 6 hours and then washed with PBS three times. The culture medium was replaced with DMEM containing 2 μM DCFH-DA and incubated for 30 min. After that, the DMEM was removed and the remaining DCFH-DA was washed three times with PBS buffer. The cells were then subjected to the photosensitization experiment with LED irradiation (50 mW cm^{-2} , 660 nm) for 5 min. Fluorescence images of DCFH-DA, staining on the cells were promptly captured by Nikon single-particle microscopy with a 40 \times objective lens.

10) $\text{O}_2^{\cdot-}$ generation in living cells

HeLa cells were seeded in 35 mm confocal dishes and incubated for 24 h under normoxia or hypoxia. Specifically, the HeLa cells were incubated with 0.5 μM **HG** at 37 $^\circ\text{C}$ for 6 hours and then washed three times with PBS buffer. The culture medium was replaced with DMEM containing 2 μM DHE and incubated for 30 min. After that, the DMEM was removed and the remaining DHE was washed with PBS buffer three times. The cells were then subjected to the photosensitization experiment with LED irradiation (50 mW cm^{-2} , 660 nm) for 5 min.

Fluorescent images of DHE, staining on the cells were promptly captured by Nikon single-particle microscopy with a 40× objective lens.

11) *In vitro* cytotoxicity

HeLa cells were seeded in 96-well plates (5×10^3 cells well⁻¹) and incubated for 24 hours under normoxia or hypoxia. Then, the medium was replaced with 100 μ L of DMEM containing different concentrations of **HG**. After incubation for another 6 hours, the cells were washed three times with PBS, infused with fresh medium, and illuminated by a LED light (660 nm, 50 mW cm⁻²) for 10 min. After further incubation for 12 hours, the cell viability was examined by cell counting kit-8 (CCK-8) assays. Moreover, the dark toxicity of **HG** was also analysed by the above procedure except the illumination was eliminated.

12) Calcein AM/PI staining of HeLa cells in PDT experiments

The HeLa cells were seeded on 35 mm confocal dishes and incubated for 24 hours. The medium was then replaced with fresh culture medium containing different concentrations of **HG** and incubated for 6 hours. Then, the culture medium was replaced with fresh DMEM containing 5 μ M Calcein AM and 5 μ M propidium iodide (PI). After further incubation for 20 min, the calcein Am and PI solution was removed and washed with PBS buffer three times. After that, the cells were irradiated with a LED light (50 mW cm⁻², 660 nm) for 5 min. Fluorescent images of Calcein AM and PI, staining on the cells, were promptly captured by Nikon single-particle microscopy with a 20× objective lens.

13) Flow Cytometry Test of Apoptosis

The HeLa cells were seeded on 6 well cell culture plate and incubated for 24 hours. The medium was then replaced with fresh culture medium containing **HG** and incubated for 6 hours. Then, the cells were irradiated with a 660 nm LED light (50 mW cm⁻²) for 10 min. After further incubation for 12 hours, the cells were collected and treated with AnnexinV-FITC/PI cell apoptosis detection kit. The flow cytometry was used to detect cell apoptosis.

14) *In vivo* imaging

Tumor imaging *in vivo* were studied with subcutaneous tumor model of human cervical cancer HeLa in the immunocompetent BALB/c mice. The tumor-bearing mice were intravenously injected of **HG** (2 mg kg⁻¹). Then, the fluorescence was recorded at different time points (1, 3, 6, 9, 12 hours) with an IVIS Spectrum imaging system.

15) *Ex vivo* biodistribution of HG

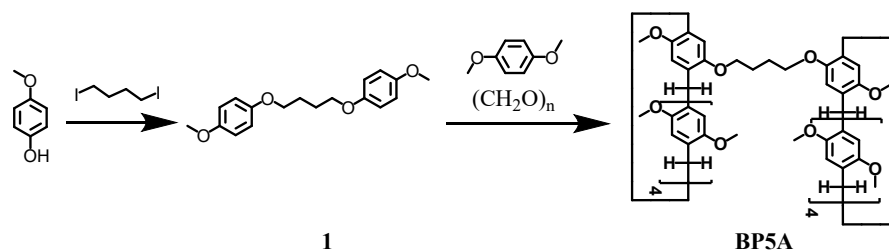
The *ex vivo* biodistribution of **HG** was evaluated at 12 hours postinjection by IVIS Spectrum imaging. Mice were sacrificed and their major organs including heart, liver, spleen, lung, kidney, pancreas, and tumor were carefully removed for visualization under the imaging system.

16) *In vivo* PDT experiment

Phototoxicity assay was performed by using HeLa tumor bearing mice. The mice were divided into three different groups for treatment: Group 1: PBS injection; Group 2: **HG** injection without irradiation; Group 3: **HG** injection with irradiation. Each group contained five mice. 6 hours and 12 hours after injection, LED light (120 mW cm⁻², 660 nm) treatment

was performed on the Group 3 by irradiating the tumor region for 20 min. The effect of the different treatment groups was monitored by measuring tumor size (tumor size = width² × length/ 2.) and mice body weight for 14 days after PDT treatment. After 14 days, the tumors were dissected and weighed.

2. Synthesis of BP5A and G



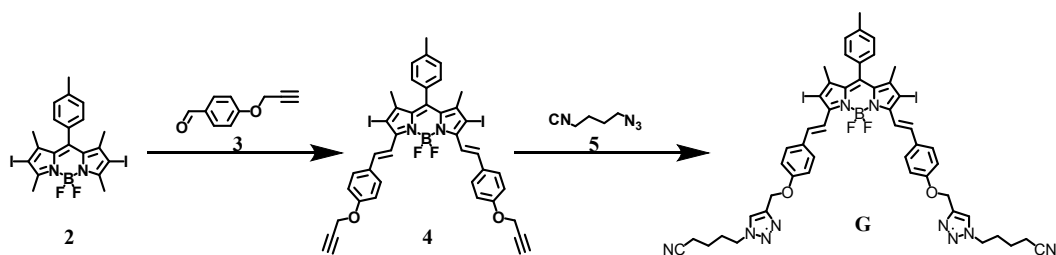
Scheme S1. Synthesis of compound **BP5A**.

Synthesis of compound **1**: 4-methoxyphenol (1.50 g, 12.09 mmol), 1,4-Dibromobutane (1.30 g, 6.04 mmol), and K₂CO₃ (4.15 g, 30 mmol) were mixed in 100 mL dry DMF and the resulting mixture was stirred at 80 °C for 48 hours. The reaction mixture was allowed to cool to room temperature. Then, 150 mL saturated brine were added to the resulting mixture. The product was extracted with ethyl acetate (3 × 150 mL) and the organic layers were combined. The organic solution was dried over anhydrous sodium sulfate and evaporated under reduced pressure. The residue was purified by column chromatography on silica gel with petroleum ether/ dichloromethane (70:30, v/v) as eluent to afford the product as white solid (2.74 g, 75%). ¹H NMR (600 MHz, Chloroform-*d*) δ 6.84 (s, 8 H), 4.02 – 3.92 (t, *J* = 5.6 Hz, 4 H), 3.77 (s, 6 H), 1.95 (t, *J* = 2.9 Hz, 4 H).

Synthesis of compound **BP5A**: Compound **1** (100 mg, 0.33 mmol) and 1,4-dimethoxybenzene (364.77 mg, 2.64 mmol) were mixed in 300 mL dry dichloromethane under N₂ atmosphere and stirred at room temperature for 0.5 hour. Then, paraformaldehyde (118.9 mg) was added to the mixture and stirred for another 2 hours. 300 mL saturated brine were added to quench the reaction and the product was extracted with dichloromethane (3 × 200 mL). The organic layers were combined and evaporated under reduced pressure. The residue was purified by column chromatography on silica gel with dichloromethane as eluent, **BP5A** as milky solid was obtained (60.5 mg, 12%). ¹H NMR (600 MHz, Chloroform-*d*) δ 6.94 – 6.63 (m, 20 H), 3.95 (s, 4 H), 3.77 (m, 20 H), 3.65 (m, 54 H), 2.05 (s, 4 H). ¹³C NMR (150 MHz, Chloroform-*d*) δ 150.98, 150.94, 150.90, 150.88, 150.86, 150.04, 128.51, 128.42, 128.39, 128.34, 128.30, 128.25, 115.03, 114.25, 114.21, 114.11, 114.07, 114.02, 67.75, 55.95, 55.89, 55.86, 55.77, 29.96, 29.83, 29.73, 29.69, 29.43, 26.94. HRMS: *m/z*; [M]⁺, calcd for C₉₂H₁₀₃O₂₀⁺: 1527.7037; found: 1527.7013.

Pillar[5]arene (**P5A**) was obtained as by-products at the same time (110 mg, 25%). ¹H NMR (600 MHz, Chloroform-*d*) δ 6.78 (m, 10 H), 3.78 (s, 10 H), 3.66 (m, 30 H).

Synthesis of compound **G**:



Scheme S2. Synthesis of compound **G**.

Synthesis of compound **4**: A Schlenk tube was charged with **2** (590.0 mg, 1.0 mmol), compound **3** (400.4 mg, 2.5 mmol). The Schlenk tube was capped with a rubber septum and then evacuated and backfilled with N_2 (this sequence was carried out two times). Glacial acetic acid (0.6 mL), piperidine (0.8 mL) and toluene (20 mL) were added via syringe through the septum, and the Schlenk tube was sealed. The reaction mixture was heated to $100\text{ }^\circ\text{C}$ for 24 hours. After the reaction mixture was cooled to room temperature, 100 mL saturated brine were added to the mixture. The product was extracted with dichloromethane (3×80 ml) and the organic layers were combined. The organic solution was dried over anhydrous sodium sulfate and removed under reduced pressure. The residue was purified by column chromatography on silica gel with petroleum ether/ dichloromethane (80:20, v/v) as eluent to afford compound **4** as fuchsia solid (375.9 mg, 43 %). ^1H NMR (600 MHz, Chloroform-*d*) δ 8.12 (d, $J = 16.6$ Hz, 2 H), 7.68 – 7.59 (m, 4 H), 7.59 (d, $J = 16.6$ Hz, 2 H), 7.33 (d, $J = 7.6$ Hz, 2 H), 7.15 (d, $J = 8.0$ Hz, 2 H), 7.03 (d, $J = 7.5$ Hz, 4 H), 4.75 (d, $J = 2.4$ Hz, 4 H), 2.56 (d, $J = 1.3$ Hz, 2 H), 2.47 (s, 3 H), 1.47 (s, 6 H).

Synthesis of compound **G**: Compound **4** (200.0 mg, 0.23 mmol), 3-azidopropanenitrile (57.1 mg, 0.46 mmol), $\text{CuSO}_4 \cdot 5\text{H}_2\text{O}$ (12.0 mg, 0.04 mmol) and sodium ascorbate (16.0 mg, 0.08 mmol) were dissolved in the mixture solution (THF/ H_2O , 40 mL, 3/1). The reaction mixture was stirred at room temperature for 24 hours. Then, the product was extracted into dichloromethane. The organic layer was dried over anhydrous Na_2SO_4 and evaporated under reduced pressure. The residue was purified by column chromatography on silica gel with ethyl acetate/dichloromethane (20:80, v/v) as eluent, and compound **G** was obtained dark purple solid (190.0 mg, 73 %). ^1H NMR (600 MHz, Chloroform-*d*) δ 8.11 (d, $J = 16.6$ Hz, 2 H), 7.69 – 7.51 (m, 8 H), 7.33 (d, $J = 7.9$ Hz, 2 H), 7.15 (d, $J = 8.0$ Hz, 2 H), 7.03 (d, $J = 8.8$ Hz, 4 H), 5.28 (s, 4 H), 4.44 (t, $J = 6.8$ Hz, 4 H), 2.47 (s, 3 H), 2.41 (t, $J = 7.0$ Hz, 4 H), 2.21 – 1.97 (m, 4 H), 1.74 – 1.63 (m, 4 H), 1.47 (s, 6 H). ^{13}C NMR (150 MHz, Chloroform-*d*) δ 171.23, 159.29, 150.42, 146.03, 144.28, 139.68, 139.31, 138.88, 133.14, 132.22, 130.21, 129.33, 128.22, 122.87, 119.04, 117.22, 115.33, 82.75, 62.15, 60.47, 49.37, 29.12, 22.42, 17.66, 16.76. HRMS: m/z ; $[\text{M}]^+$, calcd for $\text{C}_{50}\text{H}_{48}\text{O}_2\text{BF}_2\text{N}_{10}\text{I}_2^+$: 1123.2107; found: 1123.2090.

3. The ^1H NMR and 2D NMR spectroscopy of HG

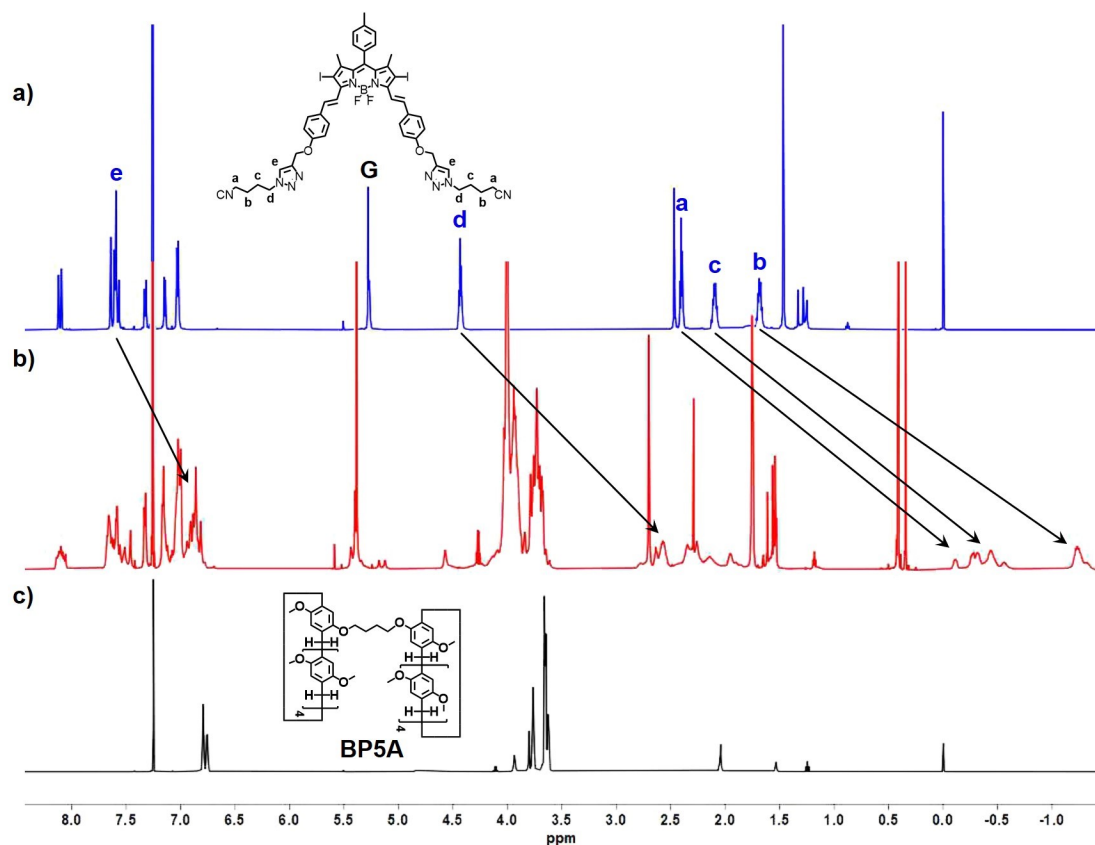


Figure S1. ^1H NMR spectra (5 mM, CDCl_3 , 600 MHz, 298 K) of a) **G** c) **BP5A**, and b) their equimolar mixture.

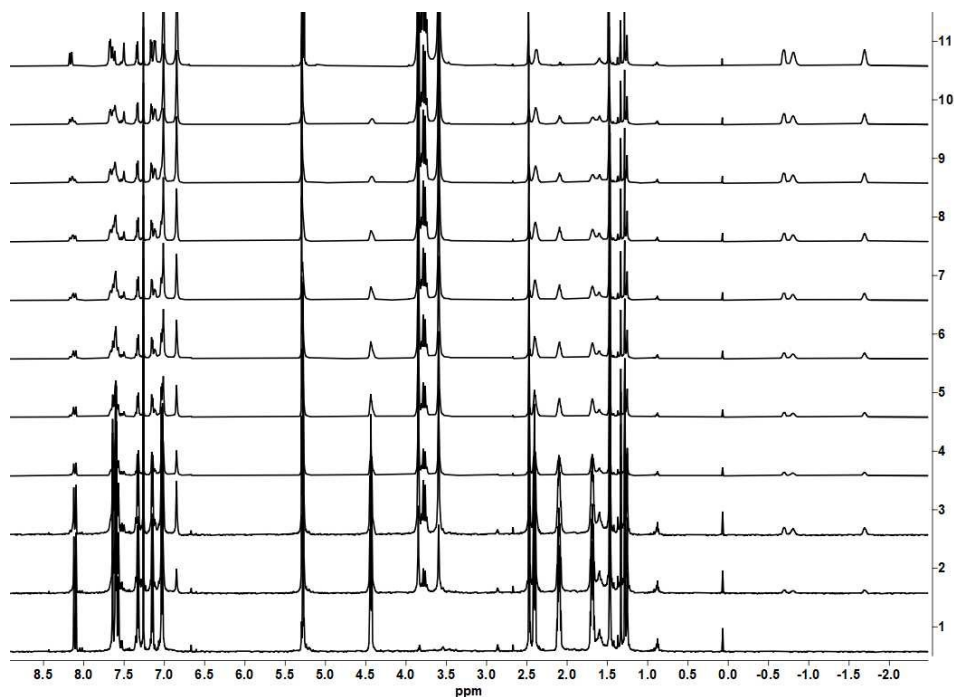


Figure S2. ^1H -NMR spectra (600 MHz, CDCl_3 , 298 K) of **G** at the concentration of 15.0 mM upon addition of **P5A**: (1) 0 mM; (2) 2 mM; (3) 4 mM; (4) 6 mM; (5) 8 mM; (6) 10 mM; (7) 12

mM; (8) 14 mM; (9) 18 mM; (10) 20 mM; (11) 30 mM.

For the present system in slow exchange on the NMR timescale, the association constant for supramolecular polymer (K_{sp}) can be calculated¹:

$$K_{sp} = \frac{[BP5A \cdot G]_c}{[BP5A]_{uc}[G]_{uc}}$$

Several solutions of equimolar mixtures of **G** and **BP5A** (0.5, 1.0 and 1.5 mM) were measured and the K_{sp} value for supramolecular polymer was determined to be $(2.2 \pm 0.4) \times 10^4 \text{ M}^{-1}$ in CDCl_3 .

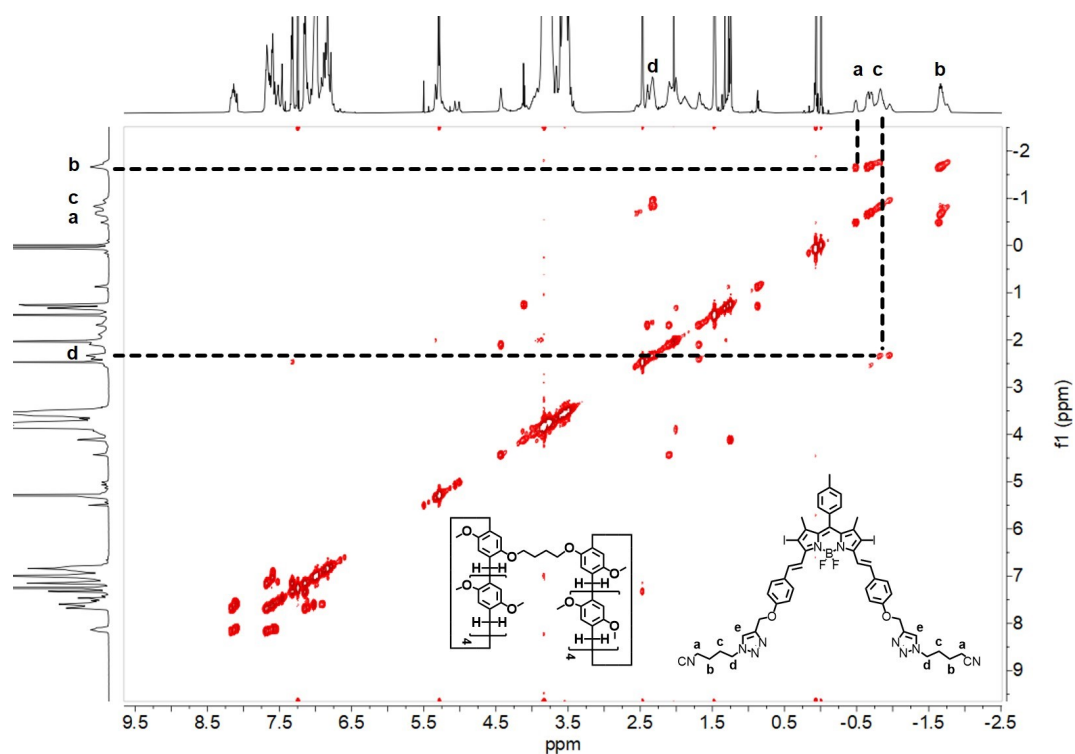


Figure S3. ^1H - ^1H COSY spectrum of equimolar mixture of **G** and **BP5A** (40 mM, CDCl_3 , 600 MHz, 298 K).

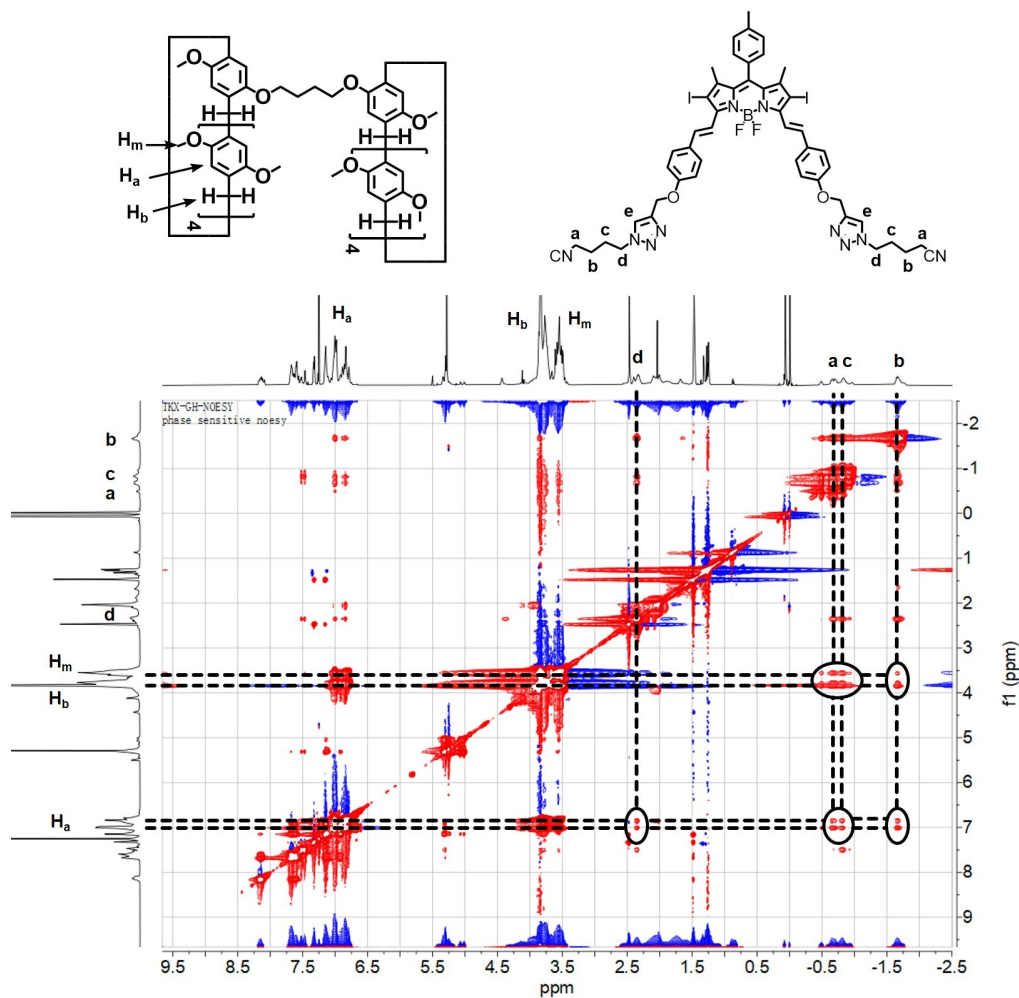
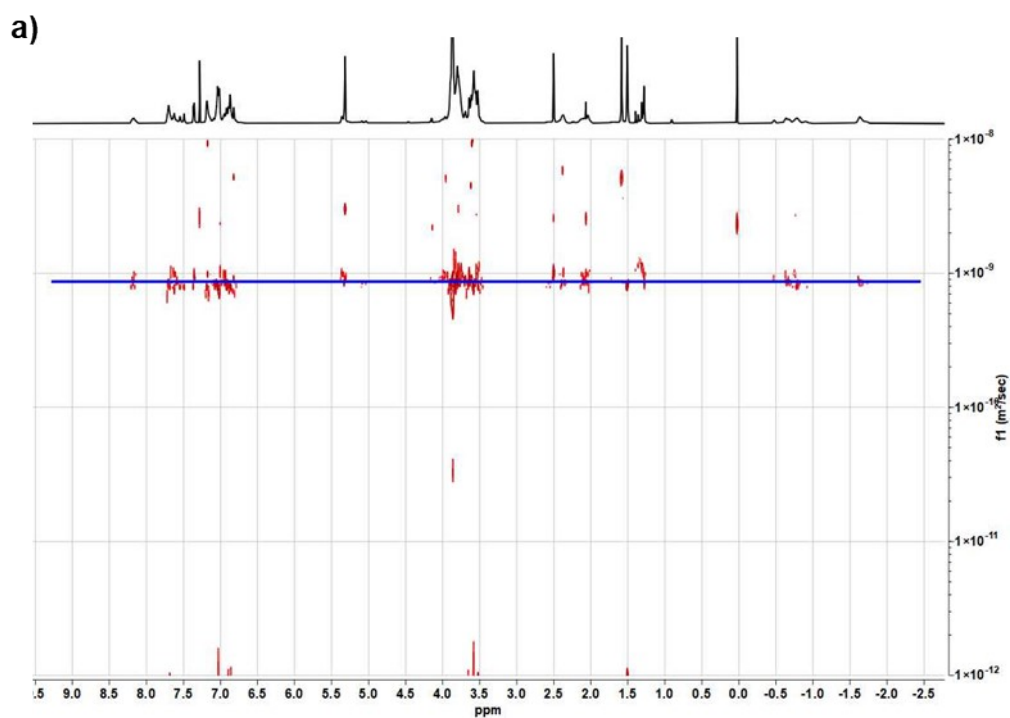
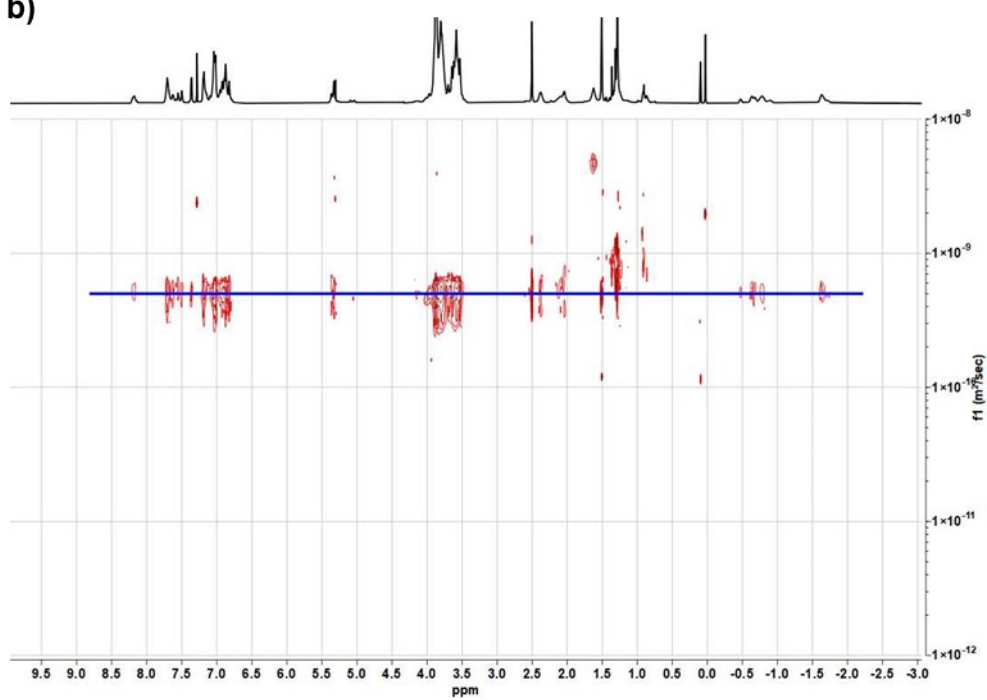


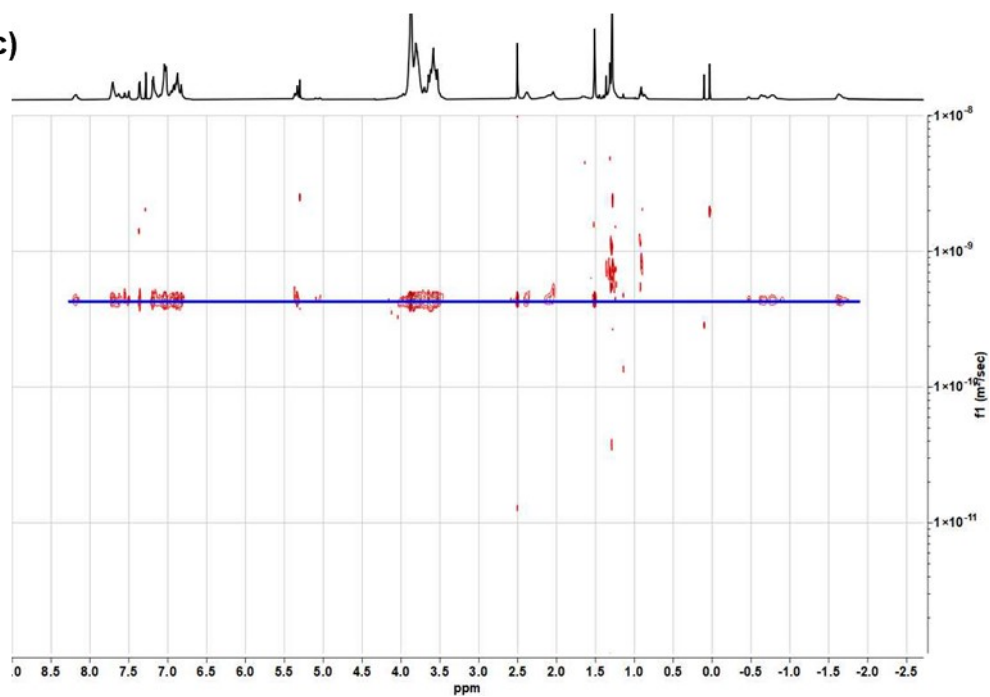
Figure S4. NOESY spectrum of equimolar mixture of **G** and **BP5A** (40 mM, CDCl₃, 600 MHz, 298 K).

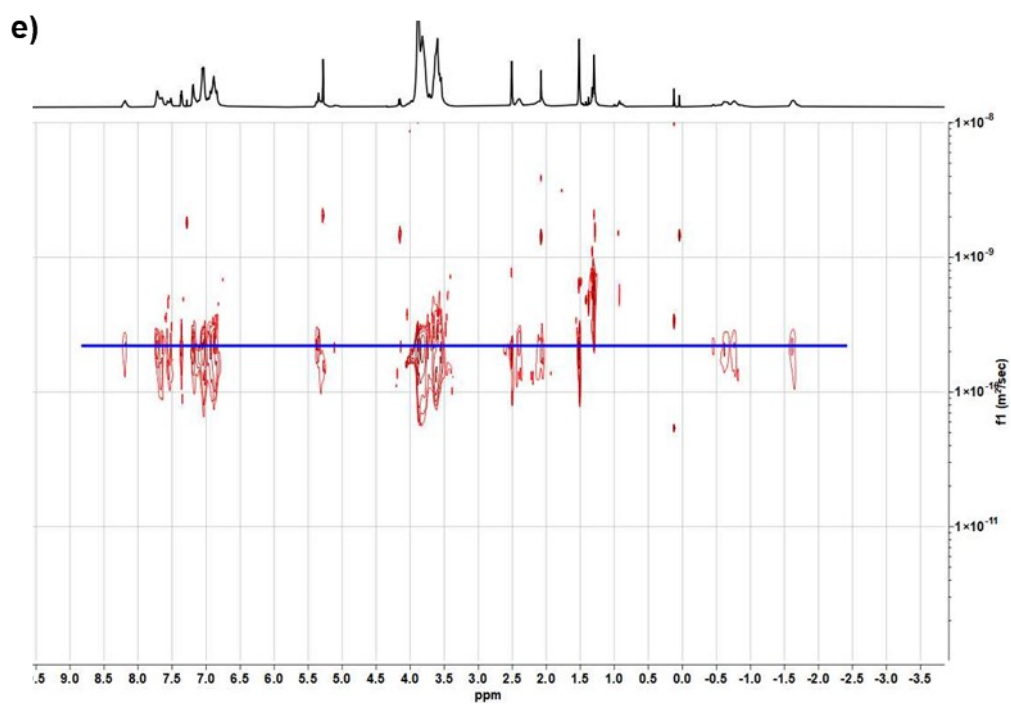
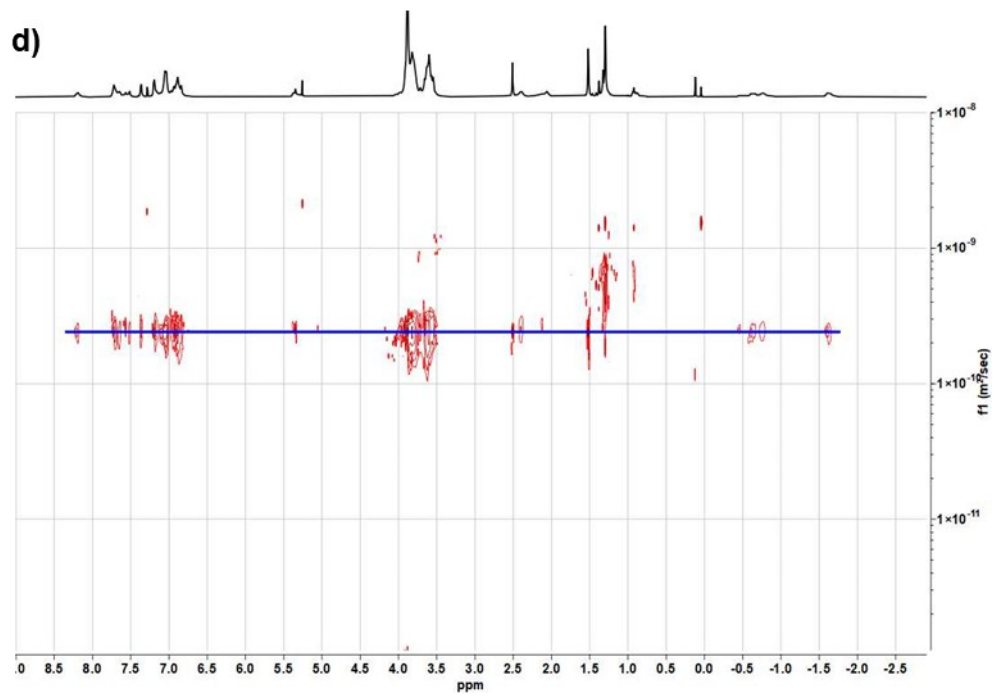


b)



c)





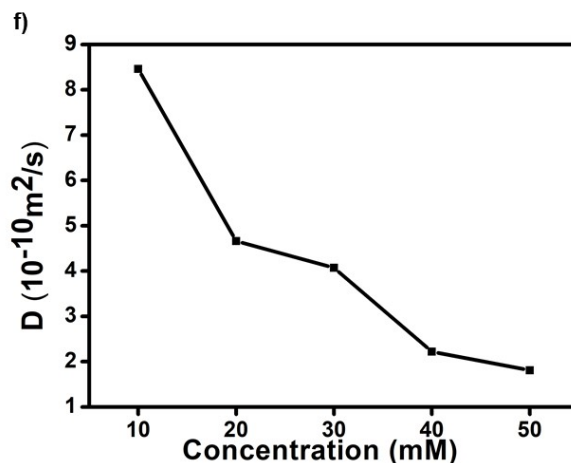


Figure S5. DOSY NMR (700 MHz, 298 K) spectra of equimolar mixture of **G** and **BP5A** at a) 10 mM; b) 20 mM; c) 30 mM; d) 40 mM; e) 50 mM. f) DOSY (700 MHz, 298 K) plots of solutions in CDCl_3 of equimolar mixture of **G** and **BP5A** at various concentrations.

4. The preparation and morphological properties of **HG**

The preparation of **HG** (Figure S6): A solution of **BP5A** (4.0 mmol, 6.2 mg) and **G** (4 mmol, 4.5 mg) in 200 μL chloroform was quickly added into deionized water with 0.9 mM cetyl trimethyl ammonium bromide (CTAB) as surfactant (10 mL). The resulting mixture was sonicated for 25 min by ultrasonic cell disruptor. After centrifuge-washing with deionized water three times, the water-dispersible nanoparticles were obtained.

The **HG** are uniformly distributed in spherical shape. The average hydrodynamic diameter of **HG** tested by dynamic light scattering was 59.2 nm, which was almost unchanged for three months at room temperature due to its excellent stability (Figure S8a). And **HG** has high photostability, which was tested remained high absorbance (> 95%) after 60 minutes of irradiation (Figure S8b). In addition, the absorption of **HG** was constant within 48 hours in fetal calf serum, indicating that **HG** were remarkably stable under physiological conditions (Figure S8c). We also prepared supramolecular nanoparticles from pillar[5]arene and **G** by the identical method (Figure S6). Compared with **HG**, these nanoparticles have a larger particle size and uncontrollable morphology, which is not conducive to subsequent applications (Figure S9b). If photosensitizer molecule without the motif of cyanoalkyl triazole was used for co-assembly with **BP5A**, no uniform nanostructure was obtained (Figure S9c). These results indicated that the host-guest interaction was crucial in assembly and formation of nanospheres.

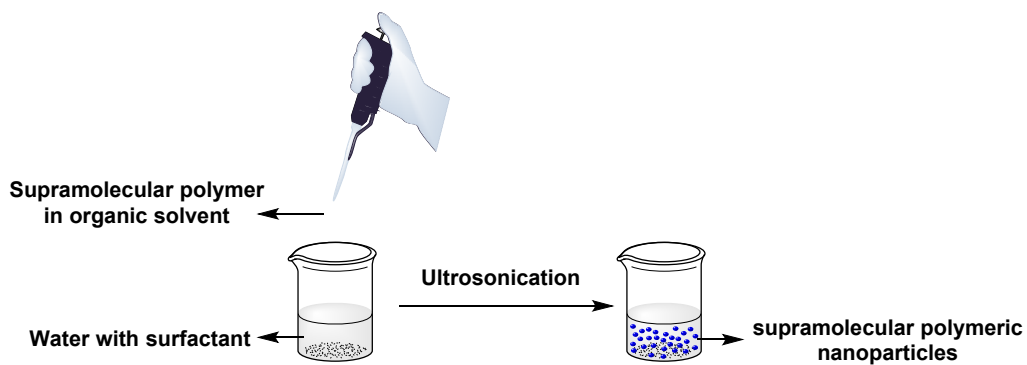


Figure S6. The scheme of the preparation of supramolecular PS nanoparticles.

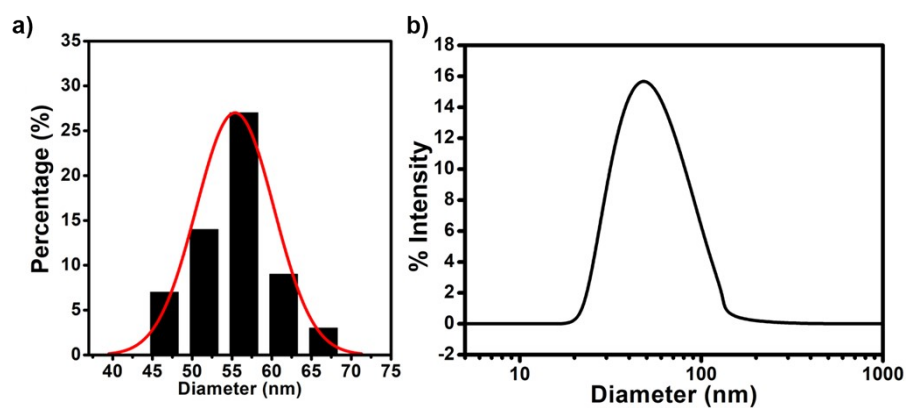


Figure S7. The particle size distribution plots of HG from a) SEM and b) DLS.

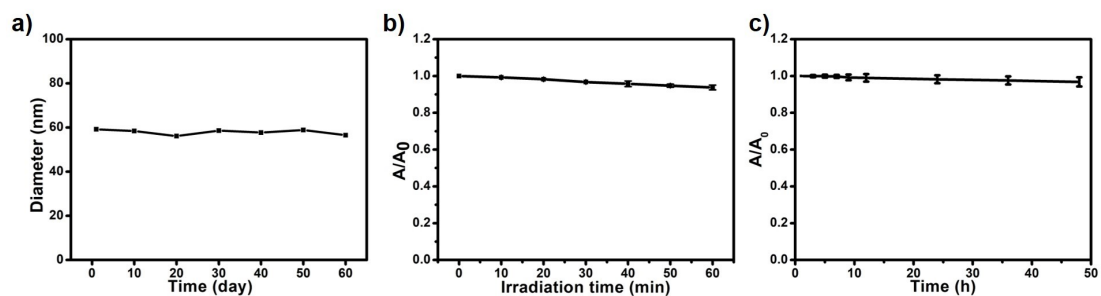


Figure S8. a) Hydrodynamic diameter of HG in PBS buffer in different days. b) The A/A_0 at 665 nm of HG at different times under the illumination of LED light (660 nm, 80 mW/cm²). c) The A/A_0 at 665 nm of HG in fetal calf serum at different times.

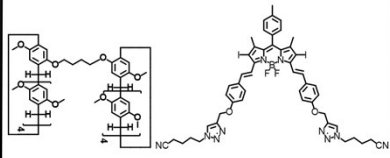

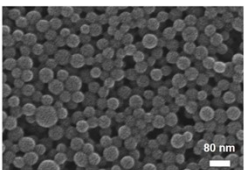
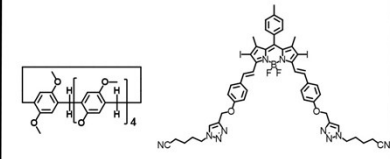
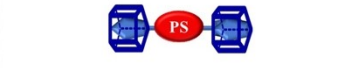
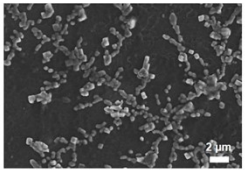
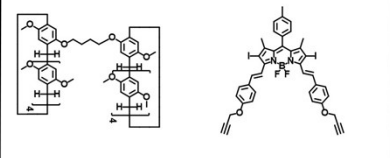

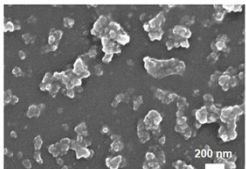
	Structure of PS and pillararenes	Schematic diagram	SEM Image
a)			
b)			
c)			

Figure S9. The SEM image of the assembly of a) **HG**; b) **G** and pillar[5]arene; c) iodide BODIPY without the motif of cyanoalkyl triazole and **BP5A**. Preparation method: A solution of pillararenes (4.0 mmol) and photosensitizer (4 mmol) in 200 μL chloroform was quickly added into deionized water with 0.9 mM cetyl trimethyl ammonium bromide (CTAB) as surfactant (10 mL). The resulting mixture was sonicated for 25 min by ultrasonic cell disruptor. After centrifuge-washing with deionized water three times, the water-dispersible nanoparticles were obtained.

5. The photophysical and photochemical properties of **HG**

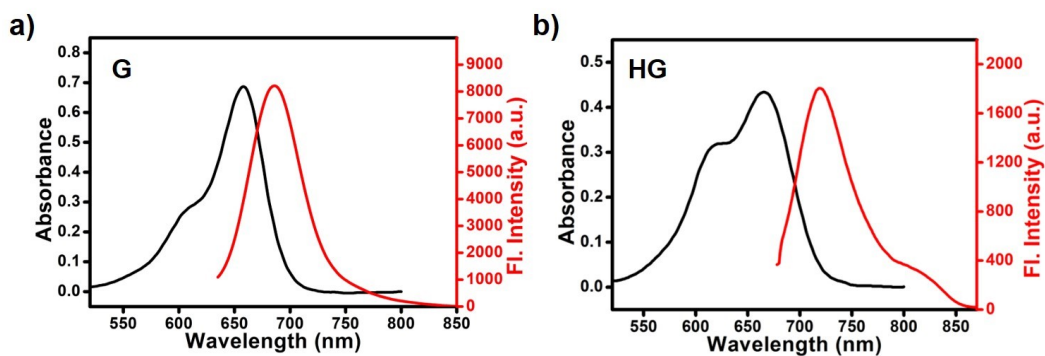


Figure S10. The absorption and fluorescence spectra of a) **G** (10 μM) in DMF and b) **HG** (10 μM) dispersed in water.

6. The evaluation of ROS generation ability

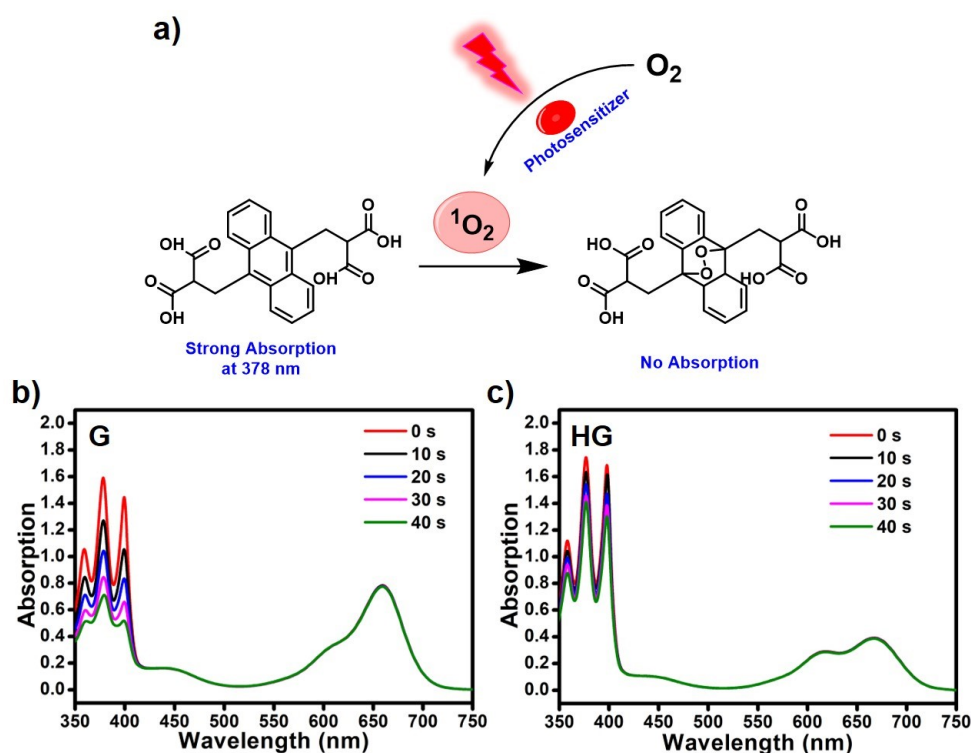


Figure S11. a) The mechanism of 9,10-anthracenediyl-bis(methylene)-dimalonic acid (ABDA) as the $^1\text{O}_2$ scavenger monitors singlet oxygen generation in the solution. The absorption spectra of ABDA ($30\ \mu\text{M}$) after irradiation ($660\ \text{nm}$, $20\ \text{mW}/\text{cm}^2$) for different time in the presence of b) **G** ($10\ \mu\text{M}$) in DMF and c) **HG** ($10\ \mu\text{M}$) dispersed in PBS.

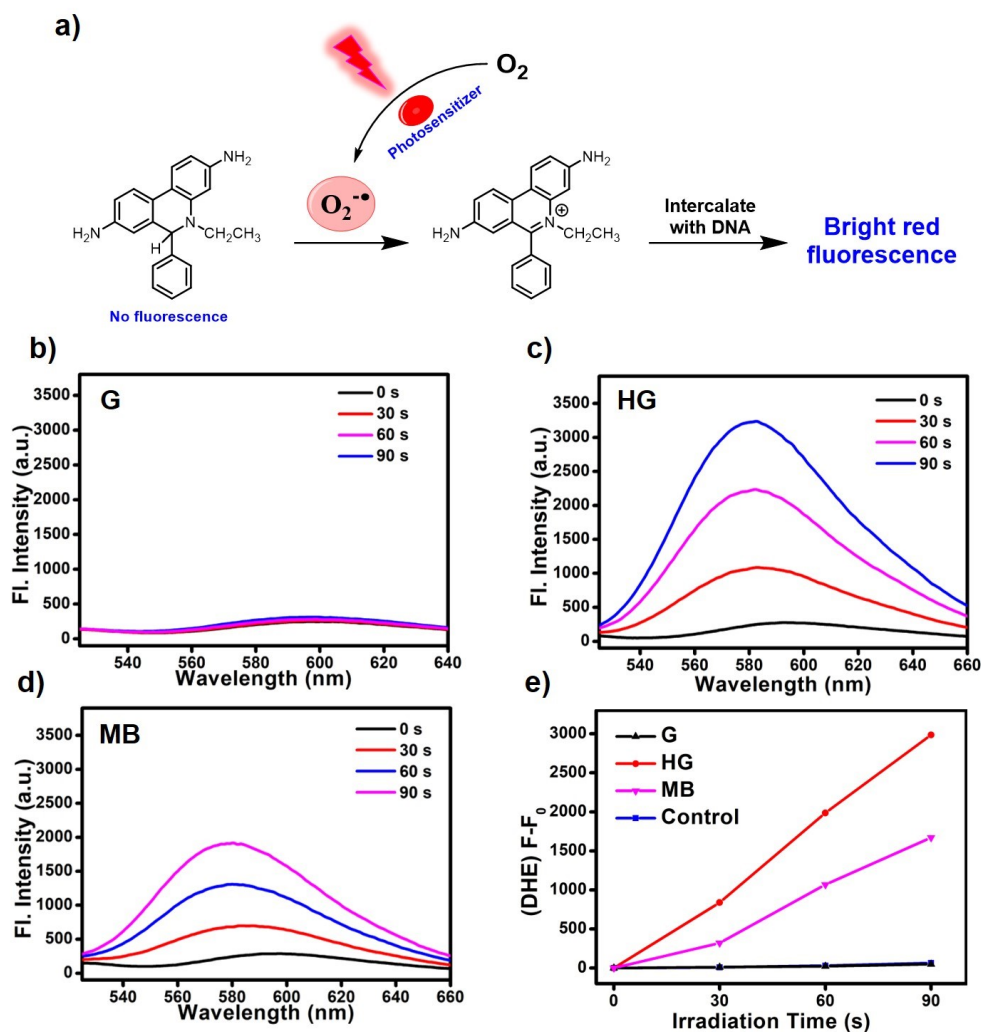


Figure S12. a) The mechanism of droethidium (DHE) as the scavenger monitors $O_2^{\cdot-}$ in the solution. The fluorescence spectra of DHE (40 μ M, excitation at 510 nm, detection from 525 nm to 660 nm) containing 500 μ g/mL ctDNA after irradiation (660 nm, 20 mW/cm²) for different time in the presence of b) **G** (10 μ M) in DMF; c) **HG** (10 μ M) dispersed in PBS and d) **MB** in PBS. e) Plots of Δ Fl. ($F-F_0$) of DHE at 580 nm upon light irradiation (660 nm, 20 mW/cm²) for different time intervals in the presence of **G**, **MB** or **HG**.

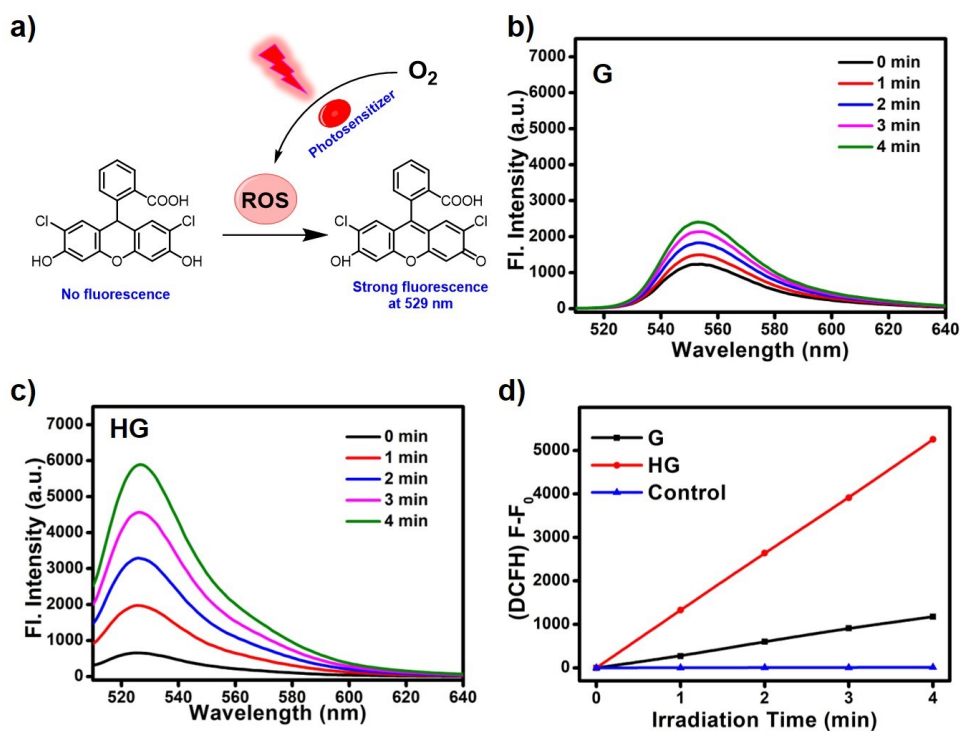


Figure S13. a) The mechanism of 2',7'-dichlorodihydrofluorescein (DCFH) as the scavenger monitors any general types of ROS in the solution. The fluorescence spectra of DCFH (40 μ M, excitation at 500 nm, detection from 510 nm to 640 nm) after irradiation (660 nm, 20 mW/cm²) for different time in the presence of b) **G** (10 μ M) in DMF; c) **HG** (10 μ M) dispersed in PBS. d) Plots of ΔF . ($F - F_0$) of DCFH at fluorescence emission maxima upon light irradiation (660 nm, 20 mW/cm²) for different time intervals in the presence of **G** or **HG**.

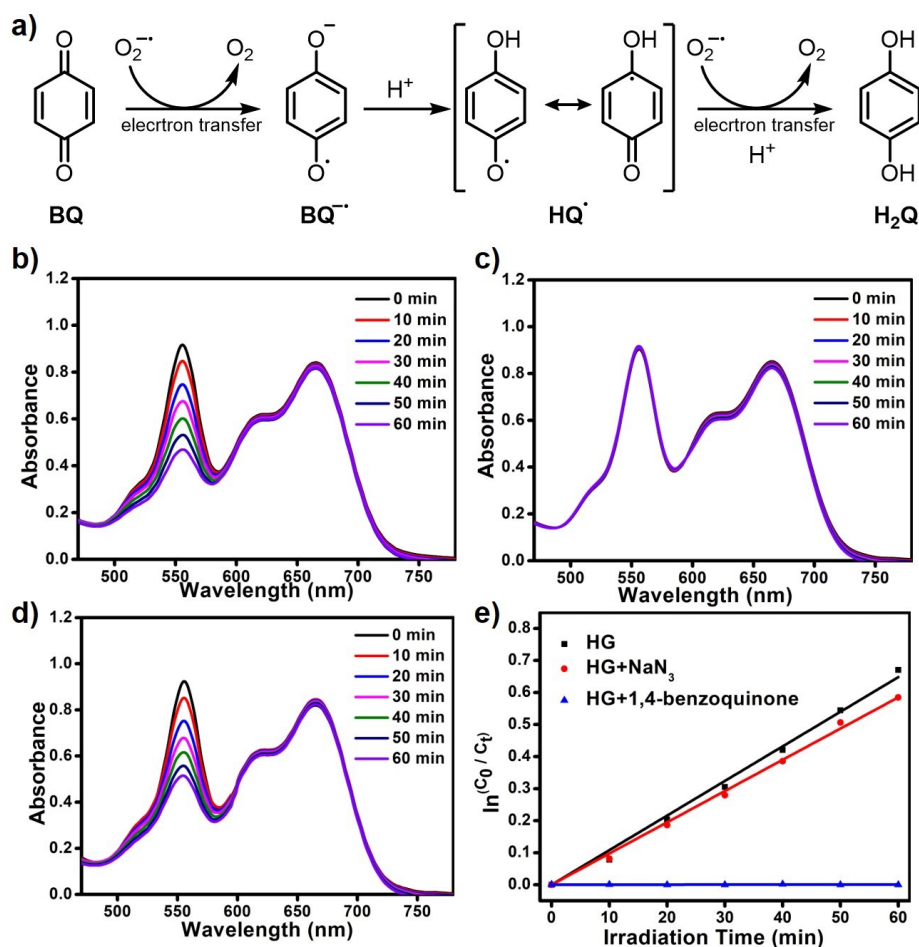


Figure S14. a) The quenching mechanism of $O_2^{\bullet-}$ by 1,4-benzoquinone.^{2,3} The absorption spectra of Rhodamine B (RhB, 10 μ M) after irradiation (660 nm, 20 mW/cm²) for different time in the presence of b) **HG** (20 μ M); c) **HG** (20 μ M) and 1,4-benzoquinone (100 μ M) as a quencher of $O_2^{\bullet-}$; d) **HG** (20 μ M) and NaN_3 (100 μ M) as a quencher of 1O_2 in water. e) First-order kinetic curves of the photodegradation of RhB under different conditions.

7. The characteristics of the aggregates of **G** and ROS generation ability

Preparation of the nanoparticles of **G**: **G** aggregates were prepared by self-assembly of **G** and Pluronic F127 through a single-step sonication method. A solution of **G** (200 μ L, 1.0 mg) and Pluronic F127 (10.0 mg) in THF was quickly added into 4 mL deionized water. Then, the resulting mixture was ultrasonicated for 25 min by ultrasonic cell disruptor. After centrifuge-washing with deionized water three times, the water-dispersible nanoparticles were obtained.

As shown in Figure S15a and S15b, the **G** aggregates were characterized by scanning electron microscopy (SEM) and dynamic light scattering (DLS). The average hydrodynamic diameter of the nanoparticles was estimated as 131.2 nm by DLS. **G** aggregates absorb at 735 nm and emits at 805 nm in water, which is significant redshifted compared to **G** and **HG** (Figure S15c and 15d). It can be seen in Figure S15e and S15f, irradiation of **G** aggregates was observed to produce a negligible amount of ROS compared to **HG**, and the amount of $O_2^{\bullet-}$ generated by **G** aggregates was also few (Figure S15g and S15h). The above results demonstrate that the aggregation of **G** cannot modulate between the Type-II and Type-I PDT mechanisms and causes the quench of the excited state, further indicating that the **BP5A** plays indispensable role for the

generation of $O_2^{\cdot-}$ by **HG**.

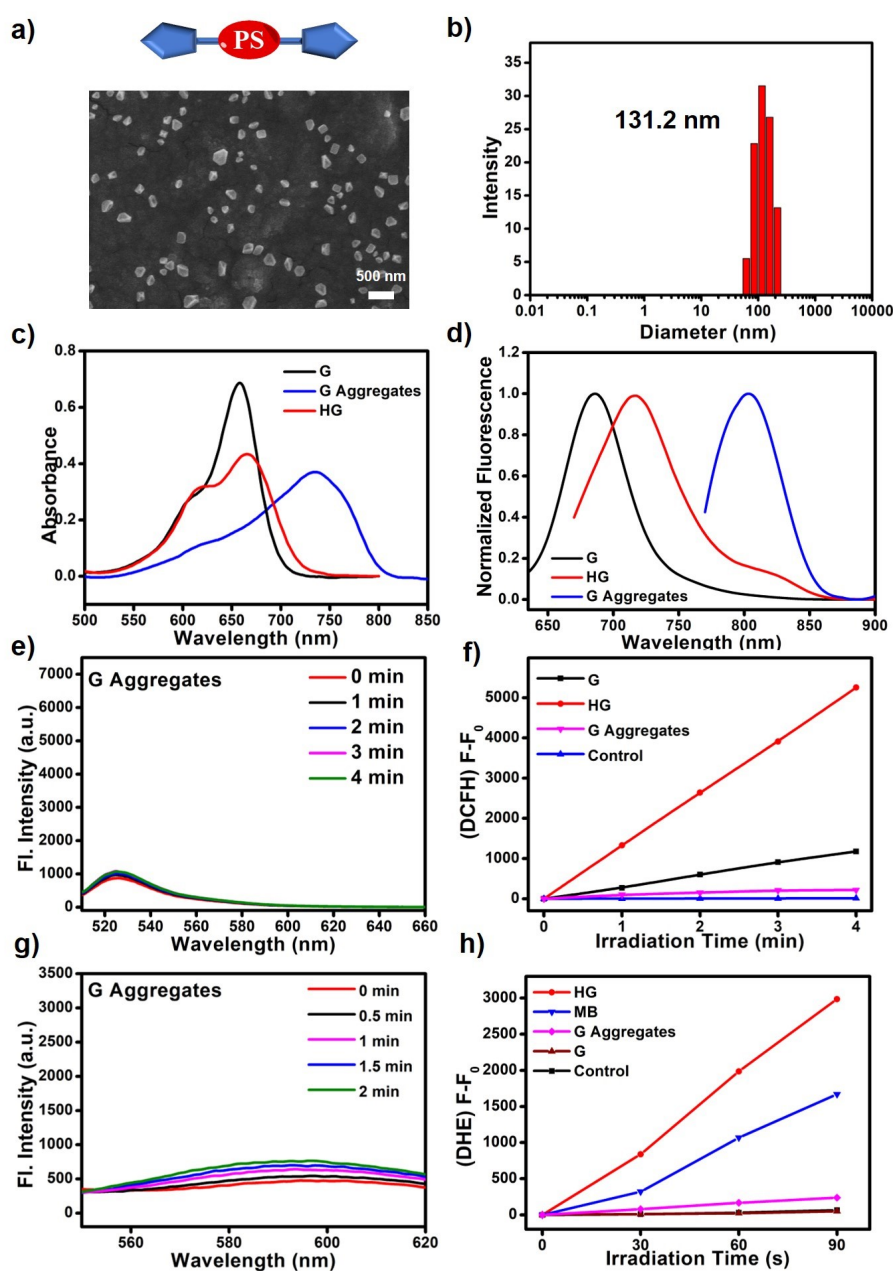


Figure S15. a) SEM image and b) DLS of the **G** aggregates. c) The absorption and d) fluorescence spectra of **G** in DMF, **G** aggregates dispersed in water and **HG** dispersed in water. e) The fluorescence spectra of DCFH (40 μ M, excitation at 500 nm, detection from 510 nm to 660 nm) after irradiation (660 nm, 20 mW/cm²) for different time in the presence of **G** aggregates (10 μ M) dispersed in PBS. f) Plots of Δ Fl. (F-F₀) of DCFH at fluorescence emission maxima upon light irradiation (660 nm, 20 mW/cm²) for different time intervals in the presence of different samples. g) The fluorescence spectra of DHE (40 μ M, excitation at 510 nm, detection from 525 nm to 620 nm) containing 500 μ g/mL ctDNA after irradiation (660 nm, 20 mW/cm²) for different time in the presence of **G** aggregates (10 μ M) dispersed in PBS. h) Plots of Δ Fl. (F-F₀) of DHE at 580 nm upon light irradiation (660nm, 20 mW/cm²) for different time intervals in the presence of different samples.

8. The electrochemical properties of G and BP5A

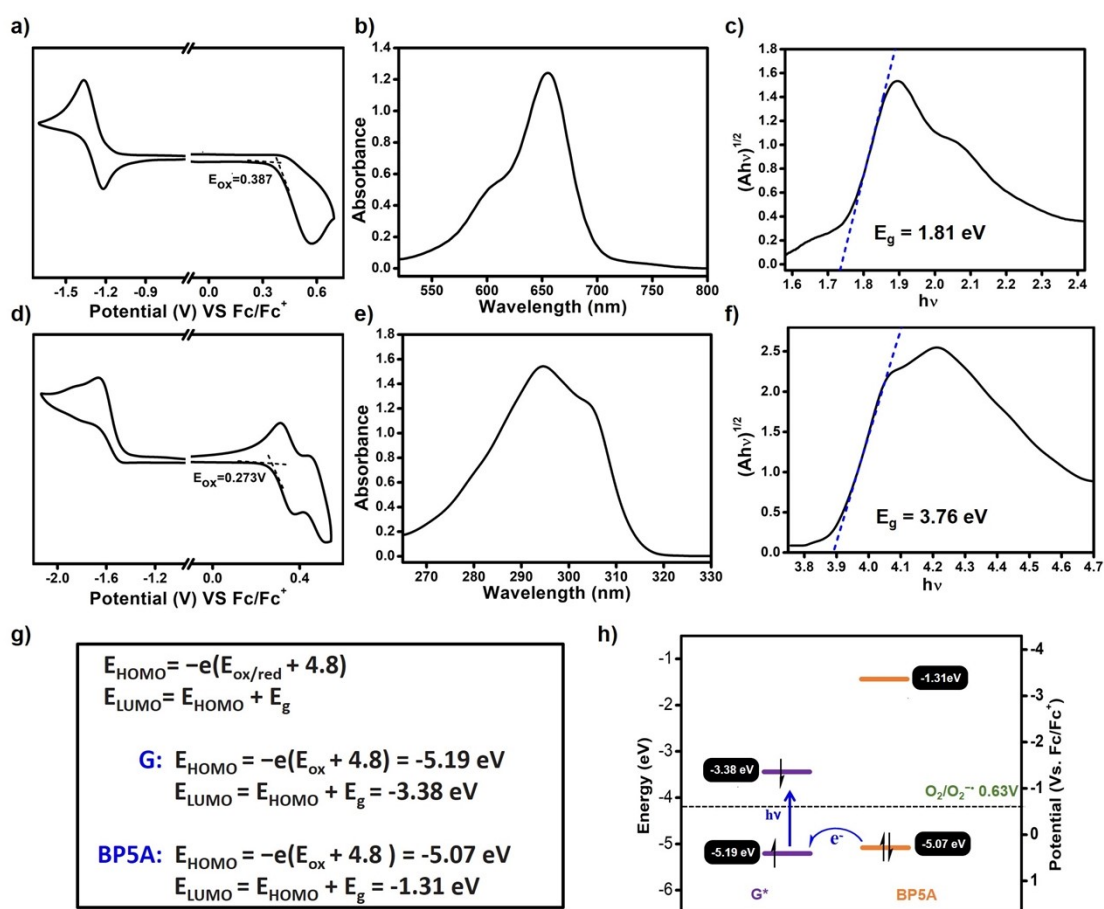


Figure S16. Cyclic voltammogram of a) **G** (1.0 mM) and d) **BP5A** (1.0 mM) in DCM with (n-Bu)₄N⁺PF₆⁻ (0.1 M) as a supporting electrolyte, Ag/Ag⁺ as a reference electrode, glassy-carbon electrode as a working electrode and Pt wire as a counter electrode; scan rate, 100 mVs⁻¹. The absorption spectra of b) **G** (20 μ M) and e) **BP5A** (20 μ M) in DCM. The Tauc plot of $(A\lambda\nu)^{1/2}$ vs. $h\nu$. $h\nu = 1024/\lambda$. g) The calculation formula of HOMO and LUMO energy levels. h) Schematic diagram of electron transfer process between **G** and **BP5A** through HOMO and LUMO energy levels.

9. Experimental data *in vitro* and *in vivo*

The cellular uptake of the supramolecular PS was tested in HeLa cells. As shown in Figure S17, the fluorescence continued to increase in NIR channel with prolonging the incubation time and reached the maximum at 6 hours, indicating that **HG** could be internalized by HeLa cells.

It can be seen in Figure S18a, obvious fluorescence signal was detected in tumor position after 6 hours for intravenous injection, which is attributed to the enhanced permeability and retention (EPR) effect. At 12 hours after the injection, the *ex vivo* biodistribution of the PS showed that the fluorescence in the tumor was stronger than that in other organs (Figure S18b). Then, we evaluated the antitumor efficiency of **HG** for HeLa tumor-bearing immunocompetent BALB/c mice (primary tumor volume: $\sim 120 \text{ mm}^3$). The **HG** was injected into the mice by tail vein injection, and irradiation (660 nm LED light, 120 mW/cm^2) was employed at 9 hours post injection. The body weights (Figure S19a) and tumor volumes (Figure S19b) were recorded during the subsequent 14 days. The weight of the mice fluctuated slightly, suggesting the negligible systemic cytotoxicity of **HG**. Moreover, the tumor volume and weight of the treatment group were significantly smaller than that of the control group, indicating that **HG** has the effect of inhibiting tumors *in vivo* (Figure S19c and S19d).

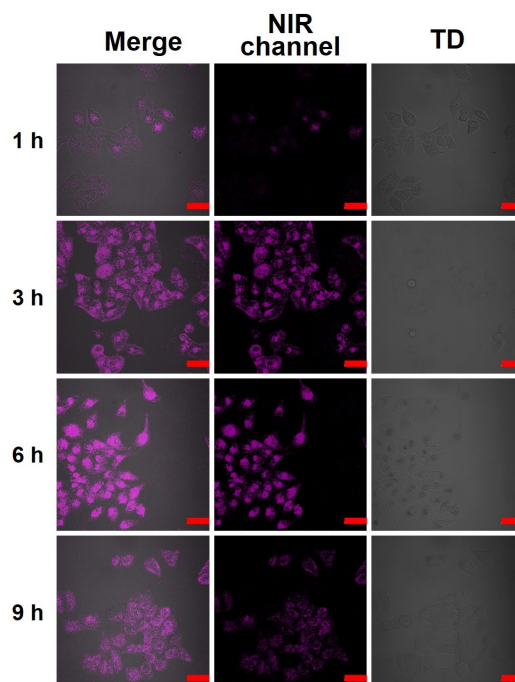


Figure S17. CLSM images of HeLa cells incubated with **HG** ($2.0 \mu\text{M}$) at different time points. The scale bar represents $50 \mu\text{m}$.

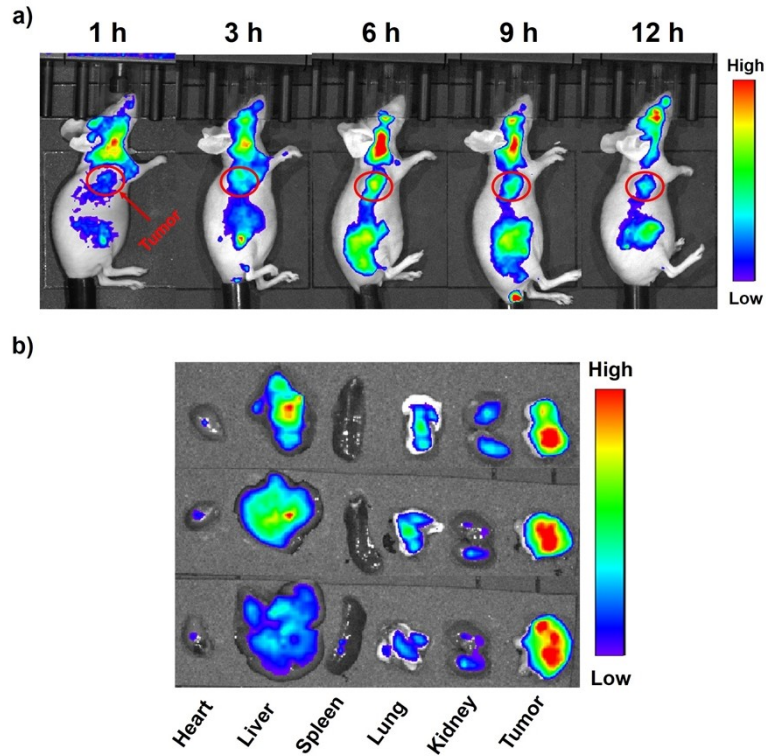


Figure S18. a) *In vivo* fluorescence imaging of HeLa tumor-bearing BALB/c mice after intravenous injection of **HG** (2 mg kg^{-1}). b) Fluorescence images of *ex vivo* organs harvested at 12 hours postinjection.

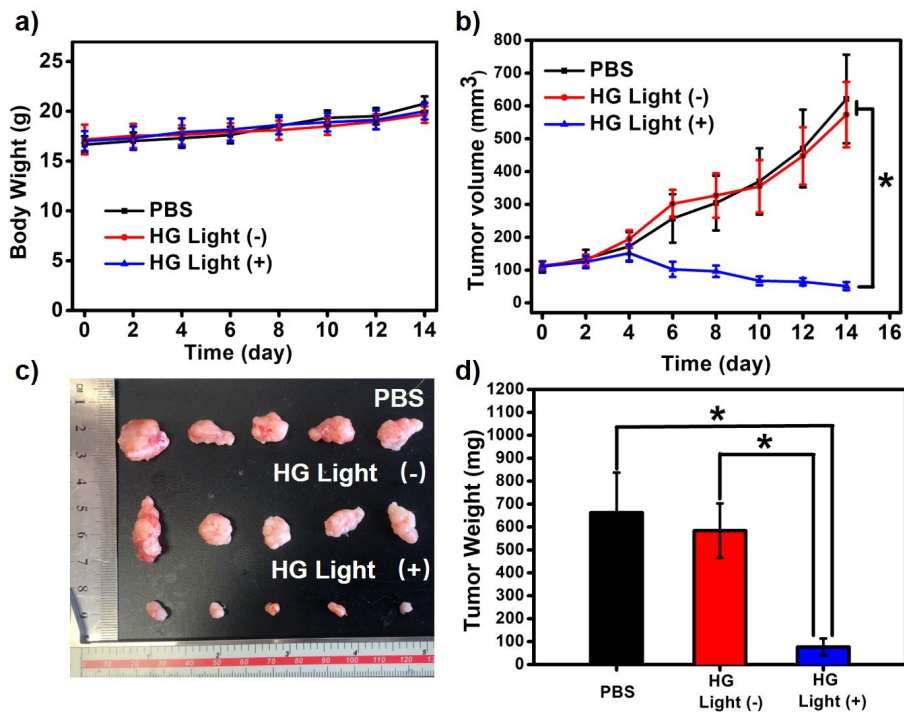


Figure S19. a) Body weights of the mice during the observation. b) Tumor growth profiles during the observation. * $P < 0.05$ (one-way ANOVA). c) Images of tumor tissues from different groups of tumors bearing mice. d) Average tumor weight of different groups of tumor-bearing mice.

10. NMR spectra and HRMS

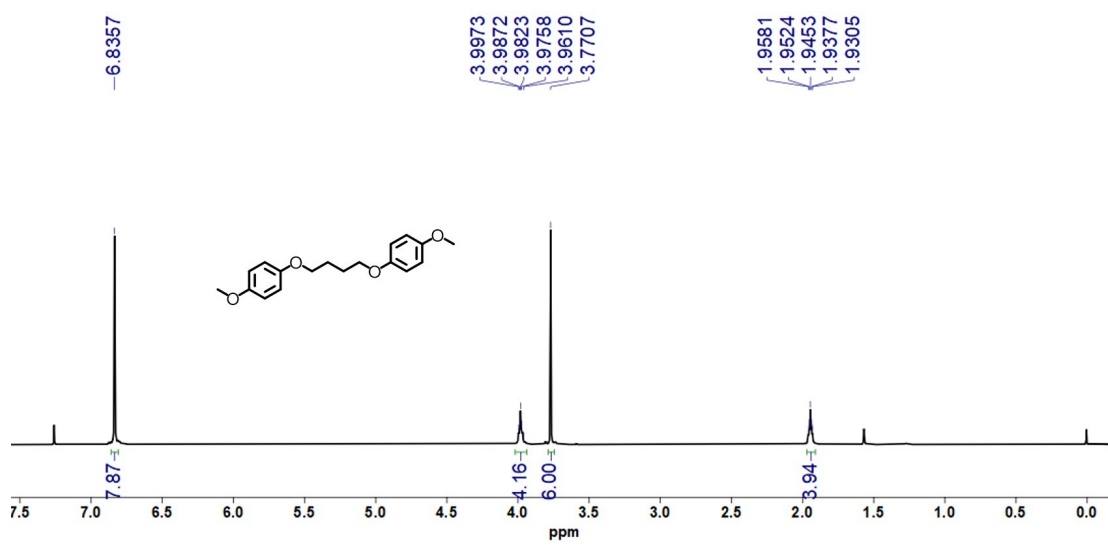


Figure S20. The ^1H NMR of compound **1** in CDCl_3 .

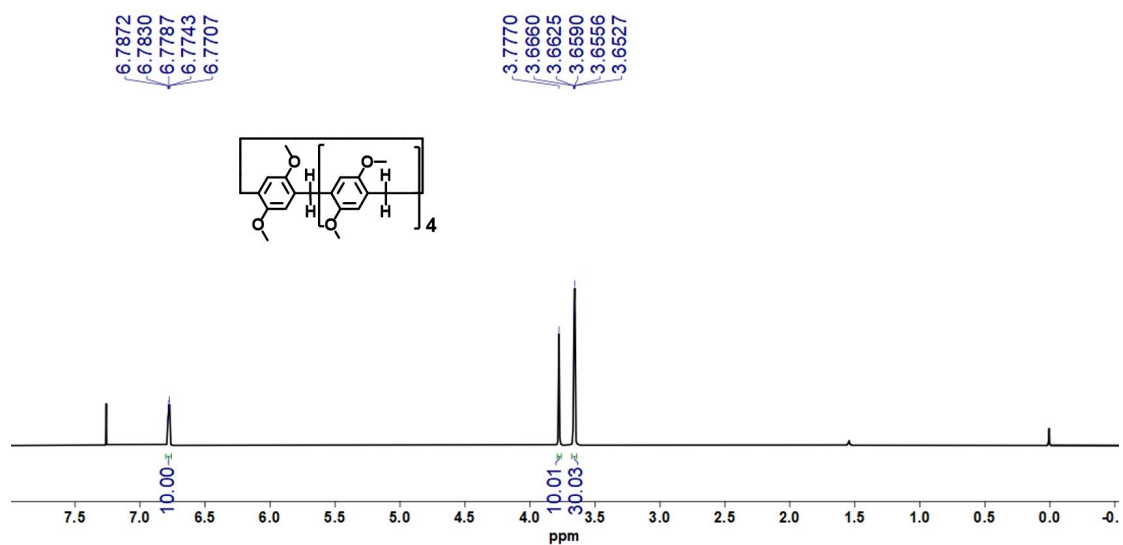


Figure S22. The ^1H NMR of pillar[5]arene in CDCl_3 .

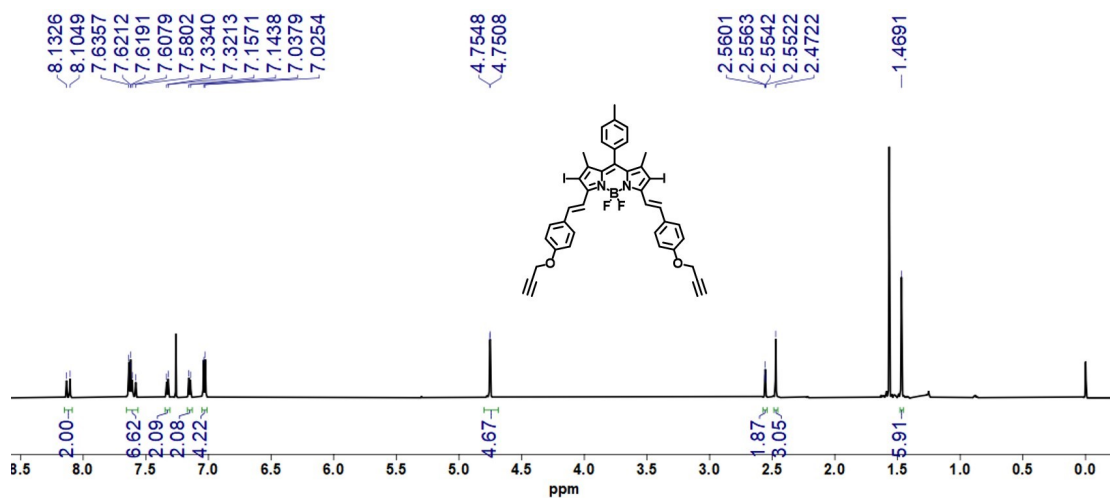
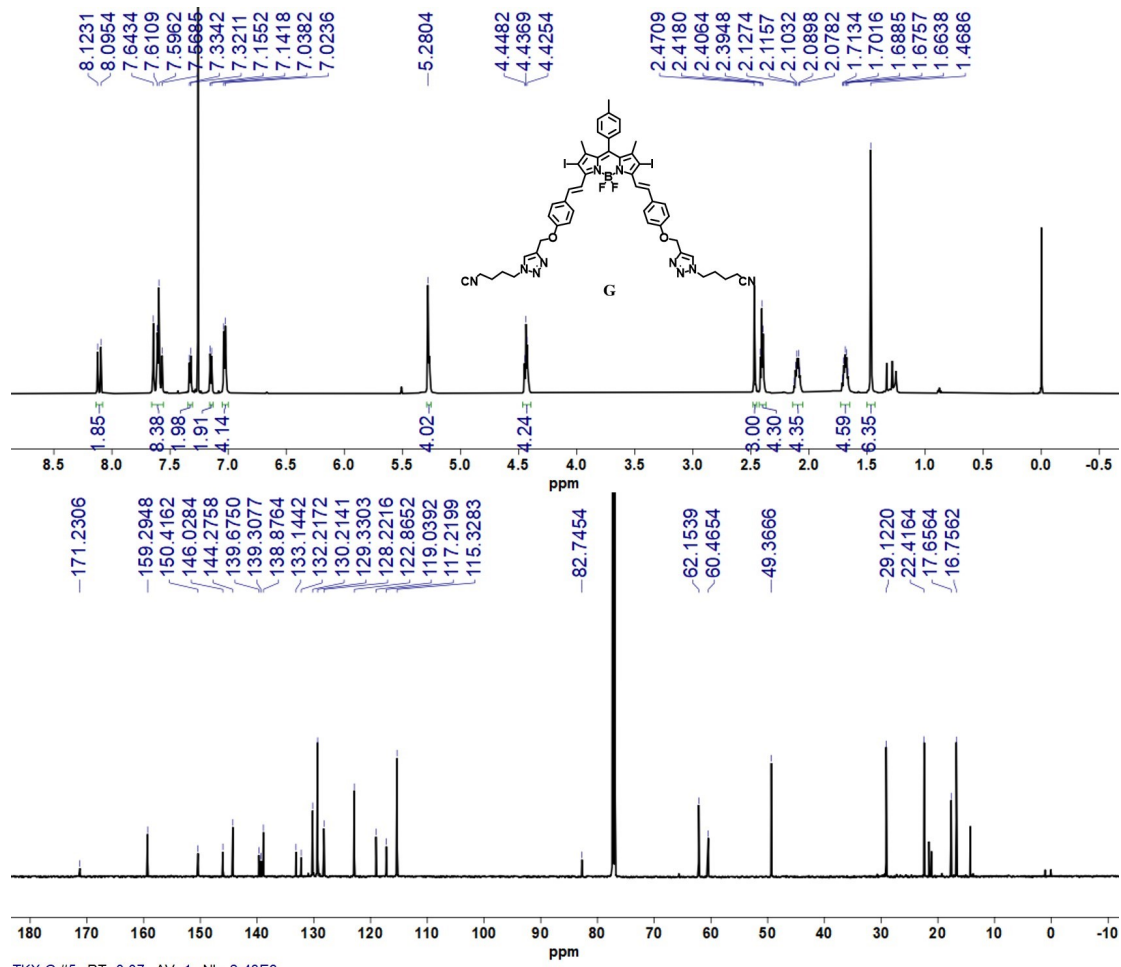


Figure S23. The ^1H NMR of compound 4 in CDCl_3 .



TKX-G#5 RT: 0.07 AV: 1 NL: 2.48E6
 T: FTMS (1,1) + pAPCI corona Full ms [200.00-2000.00]

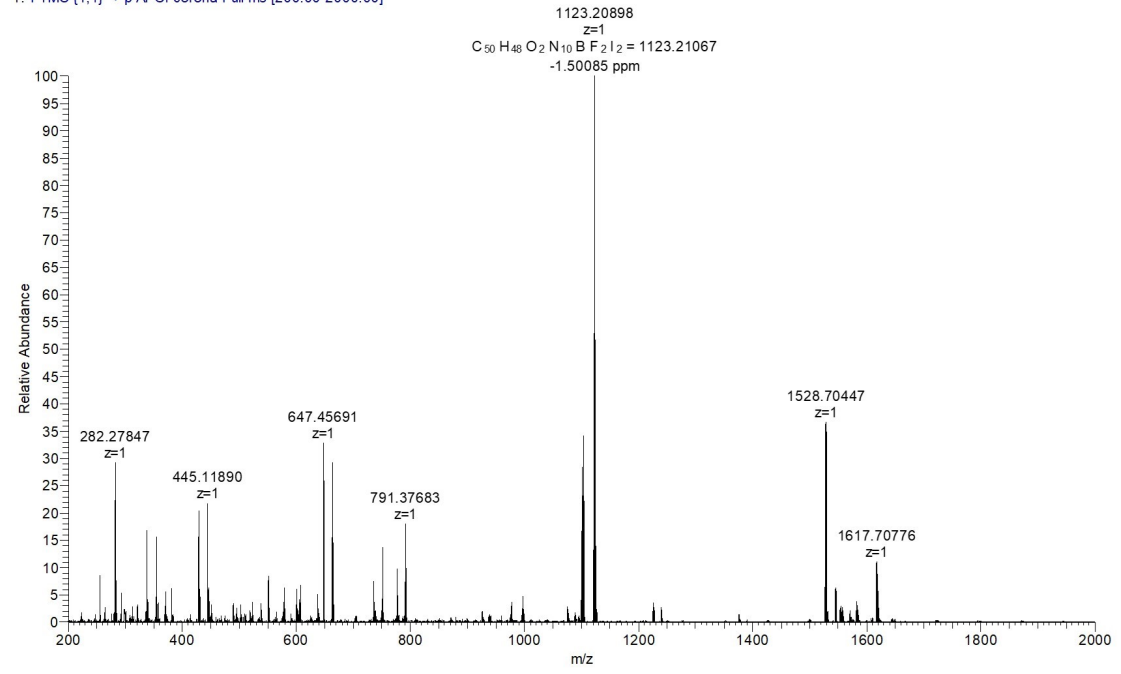


Figure S24. The ¹H NMR, ¹³C NMR in CDCl₃ and HRMS of **G**.

11. References

1. Li, C.; Han, K.; Li, J.; Zhang, Y.; Chen, W.; Yu, Y.; Jia, X., Supramolecular Polymers Based on Efficient Pillar[5]arene—Neutral Guest Motifs. *Chem.–Eur. J.* 2013, **19**, 11892-11897.
2. P. Zhang, L. Liu, X. He, X. Liu, H. Wang, J. He and Y. Zhao, Promoting Surface-Mediated Oxygen Reduction Reaction of Solid Catalysts in Metal–O₂ Batteries by Capturing Superoxide Species. *J. Am. Chem. Soc.*, 2019, **141**, 6263-6270.
3. M. Zhu, J. Lu, Y. Hu, Y. Liu, S. Hu and C. Zhu, Photochemical reactions between 1,4-benzoquinone and O₂^{•-}. *Environ. Sci. Pollut. Res.* 2020, **27**, 31289-31299.